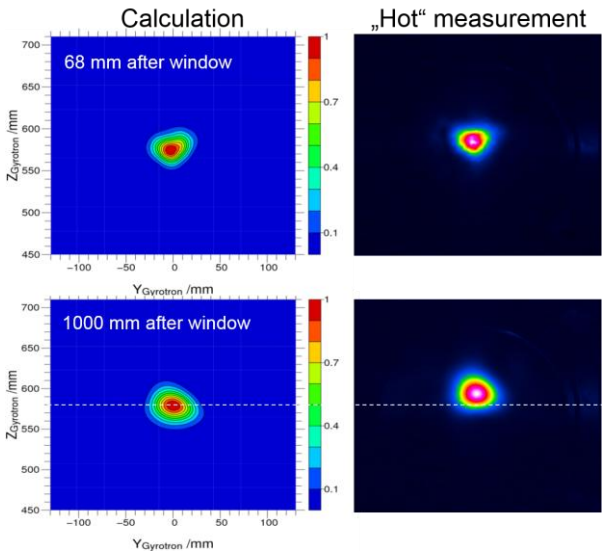

Fig. 3. Intensity distribution of the calculated and measured (IR-image) gyrotron RF output beam in 68 mm and 1000 mm distance from the window [21] (qualitative comparison).

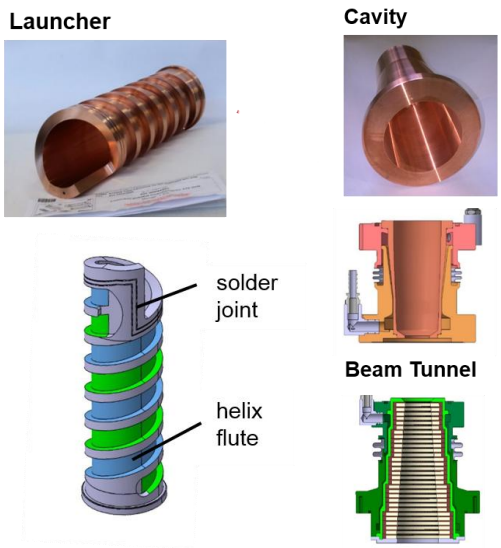

Fig. 4. Water-cooled subcomponents of the KIT 170 GHz 2 MW coaxial cavity gyrotron for pulse lengths up to 1 s.

3 Design and Manufacturing of the Coaxial-Cavity Longer Pulse Pre-Prototype Gyrotron

In order to increase the pulse length from the ms-range up to the range of one second, the main components of the 2 MW coaxial-cavity gyrotron such as the beam tunnel, the cavity, the launcher, the mirrors, the chemical vapor deposited (CVD) diamond RF output window and the collector have to be equipped with an active cooling system. The corresponding design activity was starting in 2015. The already manufactured main components of the tube are shown in Fig. 4. One of the main project requirements is to keep the modularity of the gyrotron. Therefore, an independent cooling system for each component is considered. This allows the monitoring of the internal losses in each gyrotron component and of the final energy balance of the tube during longer-pulse operation. In the following, the advanced key components of the gyrotron are described.

3.1 Inverse Magnetron Injection Gun

A major step towards higher output power and operating frequency is the Inverse Magnetron Injection Gun (IMIG) [10]. An IMIG has been designed and already manufactured for the KIT 2 MW coaxial-cavity gyrotron [22]. It is expected that this gun leads to a more stable operation at even higher output power due to the avoidance of potential wells and secondary electrons. Due to the triode configuration of the IMIG, including a separate modulation anode, the IMIG has the flexibility to be operated at multiple frequencies such as 170 GHz and 204 GHz. Because of the possibility of larger emitter radius the gyrotron can be operated at a larger operating beam current and therefore at a higher RF output power. The requested electron beam parameters are presented in Table 1 together with the operation parameters of the tube. The simulated parameters of the IMIG indicate a high electron beam quality [10], which promises a reliable gyrotron operation at nominal operating parameters. Additionally, the IMIG is the first MIG which fulfils the design criteria for preventing the generation of trapped electrons as presented in [23]. In the existing IMIG design the emitter radius is set to 62 mm with an emitter thickness of 5 mm. The emitter has an angle of 25° with respect to the z-axis of the tube. In order to keep the temperature in the neighbouring regions of the emitter low at both edges, isolation gaps with a width of 200 µm are designed. As a result, the electrons, emitted from the emitter edges have a very high pitch factor, which is related to the field enhancement at the emitter edges. In order to mitigate this effect, the emitter is pushed into the cathode by 70 µm to reduce the local electric field at the edges.

In order to minimize mechanical shifts and misalignments caused by thermal effects, the thermo-mechanical behaviour of the IMIG was investigated by the use of COMSOL. In comparison to the “conventional” MIG (Fig. 6), the cathode and emitter of the IMIG (Fig. 5) are placed at the outside of the whole structure. Hence, it is directly cooled by passing oil at the outer surface of the cathode elements. That is the major benefit if comparing to the standard MIG used in all conventional gyrotrons. The components of the cathode and anode are made of materials with high thermal conductivity, mainly CuCrZr (indicated in Fig. 5 using orange colour) and Molybdenum (Fig. 5, marked by dark blue colour). Therefore, the heat loading of the neighbouring emitter regions is directly guided outside of the MIG and absorbed by the oil flow. Compared to conventional MIGs the temperature of the loaded parts is significantly reduced by 40 % down to ~150 °C. Corresponding simulation results are presented in [24].

Another significant influence on the beam quality, hence on the generated output power and efficiency, is caused by an inhomogeneous temperature distribution at the surface of the emitter. Obviously an inhomogeneous

temperature distribution leads to an inhomogeneous emission. The emission inhomogeneity can be experimentally investigated by measuring the Current-Voltage Characteristics as published in [25]. Measurements of the temperature distribution of the emitter of the inverse MIG did indicate an azimuthal sinusoidal temperature distribution. The expected nominal temperature was 1000°C whereas the measured temperature varied between 993°C and 1007°C. One explanation for the non-constant azimuthal temperature distribution is the fact that the ends of the heater filament are not overlapping each other.

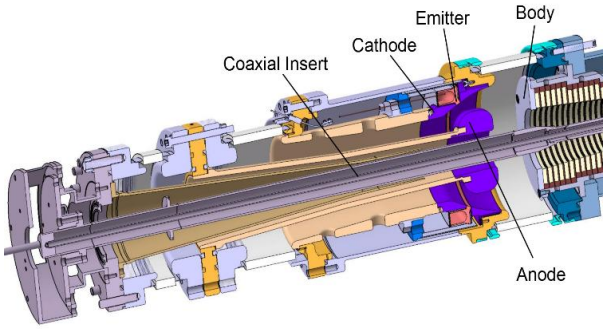

Fig. 5. Sketch of the already manufactured inverse magnetron injection gun (IMIG); the total length of the displayed section is approximately 700 mm.

3.2 Advanced Conventional Magnetron Injection Gun

The enhancement of the electric field at the emitter edges has a significant influence regarding the electron beam quality. Tolerance studies of the radial emitter position have confirmed those observations and have shown that manufacturing tolerances of some microns already become critical. A possible solution for this major issue is the implementation of an anti-emission coating at the edges of the emitter. For example, considering a misalignment of ±80 µm, the variation of the pitch factor measured over the emitter area is 83.3 % smaller compared to the variation using a conventional emitter [23]. A new conventional MIG with an advanced coated emitter for the 170 GHz 2 MW longer-pulse coaxial-cavity gyrotron, as shown in Fig. 6, has been designed by KIT and manufactured by Thales Electron Device (France) and is now available for experiments [11].

3.3 Beam Tunnel

The beam tunnel consists of alternating stacked copper rings and rings of lossy ceramics. Compared to the other components of the gyrotron, the thermal loading is relatively low; however, an active cooling is also considered for this component (see Fig. 4), which will allow to estimate the losses in the ceramic discs caused by RF stray radiation and spurious oscillations in the beam tunnel, if present.

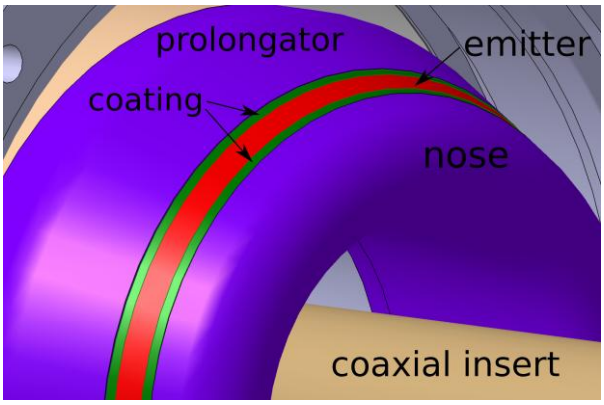

Fig. 6. Cathode of the advanced conventional magnetron injection gun (MIG) with an anti-emissive coating at the emitter edges (indicated in green).

3.4 Cavity

In the gyrotron cavity, the perpendicular kinetic energies of the individual electrons of the electron beam are transferred to the electromagnetic field. The expected total power loss in the cavity due to thermal wall loading is about 50 kW at nominal 2 MW gyrotron operation. Due to the high quality factor of the cavity one finds the peak thermal wall loading of approximately 2 kW/cm² in a very narrow region at the center of the cavity. It leads to a very high temperature gradient at the inner side of the cavity wall, which results in thermal stress, and, finally leads to a deformation of the cavity wall. Depending on that wall deformation, the operating frequency of the gyrotron is shifted and the quality factor of the cavity is changing significantly. Therefore, it is mandatory to implement effective water cooling. The chosen approach of the active cooling system is similar to the design of the cooling system for the launcher. However, due to the position and orientation, the implementation of a helix-type channel system is not necessary. The different temperatures and material properties of the coat and the outer cavity wall require also the implementation of a bellow for compensation of thermal expansion. The reduction of the water cooling gap (see Fig. 4, cavity) increases the flow velocity of the water and therefore the cooling capacity. The limitation of the cavity is a maximum temperature of approximately 350 °C. Based on this, the multi-physics software COMSOL predicts a maximum pulse length of approximately 1 s.

Additionally, the cavity uptaper is extended and optimized. The simulation results predict a transmission of 99.94 % of the $TE_{34,19}$-mode and a very low conversion to unwanted spurious modes.

3.5 Quasi-Optical Launcher

As stated before, the launcher together with the mirror system is responsible for the conversion of the cavity $TE_{34,19}$-mode into the fundamental Gaussian mode of the RF output beam [14]. Especially, at the tip of the launcher, where the complete RF-power is finally

focused, the thermal loading of 0.4 kW/cm² is critical. In order to achieve a stable operation, it is necessary to cool that launcher tip in an efficient way. To achieve that, the water inlet and outlet of the launcher is connected at the bottom of the launcher. A helix cooling structure has been used to make that configuration possible. Due to that helix structure (see. Fig. 4) the channels have to be milled with a 5-axis milling cutter. In order to caulk the channels a stainless steel coat is imposed and brazed from the outside of the launcher. The introduction of a bellow is necessary as the launcher and the coat consist of different materials that have different thermal expansion coefficients. The already manufactured launcher shows a desired surface quality. The tolerances are in the range of below ±10 µm. The launcher performance has been successfully verified in a cold measurement test setup. Fig. 7 shows the radiated pattern which was sampled at a distance of 10 cm from the axis to the position of the first mirror. The measurement results correspond well to the simulation results and the measurements on the previous launchers. The simulated radiation pattern has been calculated with the full wave 3D vector analysis code SURF3D [26]. Technologically, soldered and brazed joints with a leakage rate of $<10^{-12}$ mbar l/s were achieved for the launcher parts.

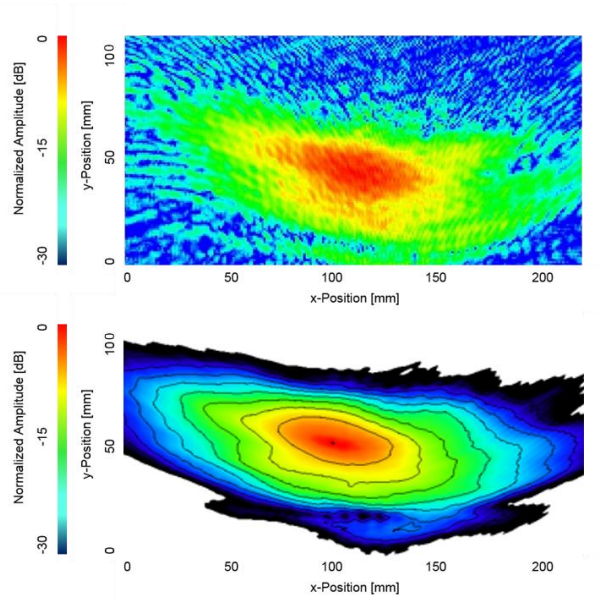

Fig. 7. Radiation pattern of the water-cooled launcher (top: cold measurement; bottom: corresponding simulation results).

4 Experimental Activities in the Near Future

During the last months, the assembly of the whole gyrotron has been finished and the tube has been equipped with a relatively old MIG for first verifications. The performed short-pulse measurements with pulse lengths ≤ 2.5 ms showed the same behaviour and output power levels as described in Section 2.

At the moment, the old MIG has been replaced by the new conventional triode type MIG with anti-emissive emitter edge coating (described in section 3.2) and new results will be expected during the next months. After finishing this measurement campaign, the experiments will be continued with the new IMIG.

5 Conclusion

KIT is pushing forward the coaxial-cavity gyrotron development by building up a modular longer-pulse 170 GHz, 2 MW pre-prototype targeting at pulse lengths of up to 1 s. The design principle and the manufacturing process of that pre-prototype have been presented here. All the subcomponents have been manufactured, brazed and successfully tested regarding vacuum tightness. Furthermore, the IMIG was manufactured at KIT with an expected high electron beam quality. Additionally, an advanced conventional MIG with coated emitter edges has been designed by KIT and manufactured at Thales Electron Devices. Both MIGs can be operated in hollow cavity as well as coaxial-cavity gyrotrons. The longer-pulse 2 MW coaxial-cavity gyrotron and the two MIGs will be tested during the next months.
Theoretical design activities are also on-going, focusing on possible two-frequency operation of the 2 MW coaxial cavity gyrotron at 170 GHz and 204 GHz [13].

This work has been carried out within the framework of the EUROfusion Consortium and has received funding from the Euratom research and training programme 2014-2018 under grant agreement No 633053. The views and opinions expressed herein do not necessarily reflect those of the European Commission. Part of the simulations was performed on the EUROfusion High Performance Computer (Marconi-Fusion).

References

1. G. Federici et al., 13th International Symposium on Fusion Nuclear Technology, 25-29 September 2017, Kyoto, Japan, to appear in Fus. Eng. Des.
2. J. Jelonnek et al., IEEE Trans. Plasma Sci., **42**, Issue 5, pp. 1135-1144. 2014, doi: 10.1109/TPS.2014.2301839.
3. J. Franck, *Systematic Study of Key Components for a Coaxial-Cavity Gyrotron for DEMO,* KIT Scientific Publishing, Karlsruhe, 2017.
4. J. Jelonnek et al., Fusion Engineering and Design, 2017, doi: 10.1016/j.fusengdes.2017.01.047.
5. H. Zohm et al., Nucl. Fusion **57**, 086002, 2017.
6. O. Dumbrajs, G.S. Nusinovich, IEEE Trans. on Plasma Science, **32**, 934-946, 2004.
7. B. Piosczyk et al., IEEE Trans. on Plasma Science, 25, 460-469 (1997).
8. S. Ruess et al., in Proc. EuMW Conference 2017, Nuernberg, Germany, Oct. 2017, EuMC40-5.
9. I. Gr. Pagonakis et al., Physics of Plasmas, **23**, 083103 (2016); doi: 10.1063/1.4959113
10. S. Ruess et al., IEEE Transactions on Electron Devices, **63**, p. 2104-2109, 2016,

DOI:10.1109/TED.2016.2540298.

11. I. Pagonakis et al., 20th Joint Workshop on Electron Cyclotron Emission (ECE) and Electron Cyclotron Resonance Heating (ECRH), May 2018, Greifswald, Germany
12. T. Ruess et al., German Microwave Conference (GeMiC 2018), 12 – 14 March 2018, Freiburg, Germany, Conference proceedings (online) DOI: 10.23919/GEMIC.2018.8335085.
13. T. Ruess et al., 20th Joint Workshop on Electron Cyclotron Emission (ECE) and Electron Cyclotron Resonance Heating (ECRH), May 2018, Greifswald, Germany
14. J. Jin et al., IEEE Transactions on Microwave Theory and Techniques, **57**, No. 7, pp. 1661-1668, 2009.
15. J. Jin et al., 20th Joint Workshop on Electron Cyclotron Emission (ECE) and Electron Cyclotron Resonance Heating (ECRH), May 2018, Greifswald, Germany
16. K. A. Avramidis et al., IEEE Trans. Electron Devices, January 2018 (online) DOI: 10.1109/TED.2017.2782365.
17. P.C. Kalaria et al., International Vacuum Electronics Conference (IVEC 2018), Monterey, California, 24-26 April 2018.
18. L. Jackowski, *Advanced Vertical Collector Sweeping for High Power Gyrotrons*, Bachelor Thesis, Oct. 2017, KIT, Karlsruhe
19. W. Kdous, *Technical Design of an Advanced Vertical Collector Sweeping System for High Power Gyrotrons*, Bachelor Thesis, April 2018, KIT, Karlsruhe
20. T. Rzesnicki et al., IEEE Transactions on Plasma Science, VOL. 38, NO. 6, June 2010.
21. T. Rzesnicki et al., 34th International Conference on Infrared, Millimeter, and Terahertz Waves, Busan, 2009, doi: 10.1109/ICIMW.2009.5324919
22. T. Rzesnicki et al, in Proc. 38th IRMMW-THz, Mainz, Germany 2013, We5-3.
23. I. Gr. Pagonakis et al., Physics of Plasma, **23**, Page 023105, 2016
24. S. Ruess et al., Vacuum Electronics Conference (IVEC) 2016 IEEE International, pp. 1-2, 2016.
25. J. Zhang et al., Proc. IVEC 2015, Beijing, China, 2015.
26. J. Neilson, Joint 29th Int. Conf. on IRMMW & 12th Int. Conf. on Terahertz Elect., Karlsruhe, Germany, 2004, pp. 667-668.